ELSEVIER

International Journal of Heat and Fluid Flow 23 (2002) 13–21

International Journal of HEAT AND FLUID FLOW

www.elsevier.com/locate/ijhff

Calculation of turbulent heat flux distributions in a square duct with one roughened wall by means of algebraic heat flux models

H. Sugiyama [a], M. Akiyama [a], Y. Nemoto [a], F.B. Gessner [b,*]

[a] *Graduate School of Engineering, Utsunomiya University, 7-1-2 Yoto, Utsunomiya 321-8585, Japan*
[b] *Department of Mechanical Engineering, University of Washington, Box 352600, Seattle, WA 98195-2600, USA*

Received 10 January 2001; accepted 2 August 2001

Abstract

Calculations have been performed for fully developed turbulent flow and heat transfer in a square duct with one roughened wall. This paper focuses on the application of two algebraic models of the turbulent heat flux transport equation to predict turbulent heat flux component behavior. The convection and diffusion terms in this transport equation are modeled in a manner similar to Rodi's approximation for corresponding terms in the Reynolds stress transport equations. The pressure–temperature gradient term is simulated by means of two models: one a composite based on the "slow" and "rapid" interaction models proposed by Lumley and Launder (LL), respectively, and the other, the model proposed by Jones and Musonge (JM). Both the LL and JM models lead to predicted mean temperature distributions in the duct cross plane that are in relatively good agreement with experimentally measured distributions. The LL model, however, yields predicted distributions that agree better with experiment near both the smooth and roughened walls of the duct. Calculated turbulent heat flux component distributions in the cross plane show that both the LL and JM models predict experimentally observed features in the flow, with the LL model providing the best overall accuracy.

Keywords: Square duct flow; Rib-roughened wall; Secondary flow; Turbulent heat flux components

1. Introduction

In some square duct heat exchanger applications, one or more walls of the duct are roughened in order to enhance heat transfer between the flowing fluid and the duct surroundings. The efficiency of the process depends greatly on the nature of the roughened wall. For example, with periodically spaced, rib-type roughness elements installed normal to the primary flow direction, heat transfer across the wall is enhanced with minimal increase in pressure drop, provided that the height of the roughness elements is small compared to the duct height. Research on turbulent flow in square ducts with one or more rib-roughened walls can be classified into two types of basic studies: those concerned with local flow and heat transfer in the vicinity of a rib-roughened wall and those concerned with global flow and heat transfer behavior across the entire duct cross-section. The present study lies within the latter category, and focuses on the nature of temperature and turbulent heat flux distributions in the duct cross plane, as influenced by one roughened wall for fully developed flow conditions. In reference to previous research in this area, Humphrey and Whitelaw (1980), Fujita et al. (1988, 1989, 1990) and Yokosawa et al. (1989) have measured mean flow and turbulence properties in a square duct having one or more rib-roughened walls. The results of Fujita et al. (1989), for example, show that the overall flow pattern in a square duct with one rib-roughened wall does not depend strongly on whether measurements are made in the duct cross-section directly over a rib or midway between adjacent ribs, provided the rib height (h) compared to the duct height (H) is small ($h/H = 0.02$ for the operating conditions of that study). This conclusion provides justification for treating a rib-roughened wall as one of uniform roughness for cross-planar flow predictions when the flow is fully developed, as is done in the present study.

* Corresponding author. Tel.: +1-206-543-5046; fax: +1-206-685-8047.
E-mail address: gessnerf@u.washington.edu (F.B. Gessner).

0142-727X/02/$ - see front matter
PII: S0142-727X(01)00132-1

Nomenclature

a	thermal diffusivity
B	duct half width (Fig. 1)
C_μ	coefficient (= 0.09)
D	duct width (Fig. 1)
h	rib height
H	duct height ($H = D$ for a square duct)
k	turbulence kinetic energy
L	characteristic length
p	fluctuating static pressure
P	mean static pressure
P_k	turbulence kinetic energy production rate
Re	Reynolds number ($= U_b D/\nu$)
t	time
T_c	axial centerline temperature
T_w	wall temperature
T'	temperature fluctuation
u_i	ith fluctuating velocity component; $i = 1, 2, 3$
$\overline{u_i T'}$	ith turbulent heat flux correlation; $i = 1, 2, 3$
$\overline{u_i u_j}$	Reynolds stress tensor; $i = 1, 2, 3$
U_b	bulk velocity
U_c	axial centerline velocity
U_i	ith mean velocity component; $i = 1, 2, 3$
U_τ	friction velocity ($= \sqrt{\tau_w/\rho}$)
X_i	ith Cartesian coordinate; $i = 1, 2, 3$
X_w	wall coordinate

Greeks

ε	isotropic dissipation rate
ε_{ij}	dissipation rate tensor
κ	von Karman's constant (= 0.42)
ν	kinematic viscosity
ρ	fluid density
τ_w	wall shear stress

Special

($\overline{\quad}$) time averaged correlation

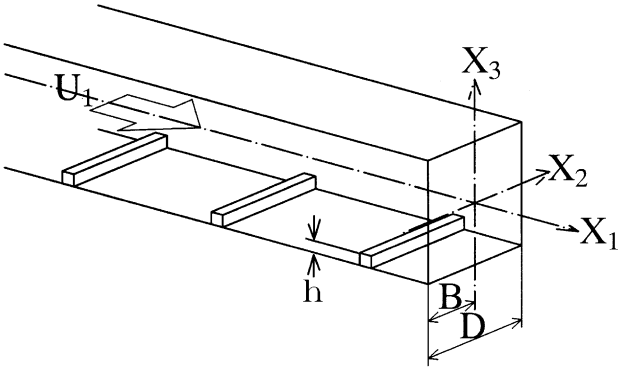

Fig. 1. Square duct with one roughened wall and definition of coordinate system.

In reference to numerical analyses of square duct flow with one roughened wall, the predictions of Sugiyama et al. (1993) are in relatively good agreement with experimental distributions measured by Fujita et al. (1989), which include primary flow velocity, secondary flow velocity, turbulence kinetic energy and Reynolds stress anisotropy distributions in the cross plane. Their turbulence model consists of transport equations for k and ε in conjunction with an algebraic stress model based on the pressure–strain model proposed Gessner and Eppich (1981) and Rodi's (1976) approximation for the convection and diffusion terms in the Reynolds stress transport equations. In a more recent study, Naimi and Gessner (1997) have shown that even better agreement with Fujita et al.'s data is possible if the Reynolds stress transport equation model developed by Naimi and Gessner (1995) is applied to a square duct flow with one roughened wall.

Heat transfer measurements and predictions in square ducts with one or more roughened walls are fairly scarce. For the case of fully developed flow and heat transfer in a square duct with either two opposite, or all four, rib-roughened walls, Fujita et al. (1988) predicted temperature contours in the duct cross plane and local wall heat flux distributions, but no comparisons with experimental data were made. In a subsequent study, Sugiyama et al. (1995) compared their predictions with experimental results presented by Hirota et al. (1994), which include mean temperature distributions in the duct cross plane, as well as local Nusselt number distributions along the smooth walls of the duct opposite and adjacent to a rib-roughened wall. In more recent work, Hirota et al. (1997), present cross planar distributions of the three turbulent heat flux components ($-\overline{u_i T'}$, $i = 1, 2, 3$), as measured in a square duct with one rib-roughened wall. Measurements such as these provide valuable data from the standpoint of assessing proposed models of the turbulent heat flux transport equation.

The precise modeling of turbulent heat flux behavior is especially important if the temperature field is to be predicted accurately in duct flows dominated by secondary flow effects (e.g., square duct flow with or without roughened walls). Furthermore, accurate modeling of the pressure–temperature gradient term in the turbulent heat flux transport equation is just as important as modeling the pressure–strain term in the Reynolds stress transport equations accurately for good predictions of the both the mean velocity and mean temperature fields. The purpose of the present study is to investigate the predictive capabilities of two algebraic versions of the turbulent heat flux transport equation

based on two different models for the pressure–temperature gradient term which appears in this equation. The flow situation considered is that of fully developed flow and heat transfer in a square duct with one rib-roughened wall. This work represents an extension of the results reported by Sugiyama et al. (1995), which did not include comparisons between calculated and measured turbulent heat flux distributions because experimental data were not available at that time.

2. Physical flow situation

The duct configuration and coordinate axes are shown in Fig. 1. The operating conditions correspond to those employed by Hirota et al. (1994, 1997). In brief, their experimental configuration consisted of a square duct, 50 mm × 50 mm in cross-section, with an overall length of 4770 mm (= 94.5D) and nominally uniform flow at the duct inlet ($X_1 = 0$). The unheated portion of the duct consisted of a 3020 mm long section, which yielded fully developed turbulent flow at the entrance to the heated section (at $X_1/D = 60.4$). This section, which consisted of 10 mm thick aluminum walls and extended from $X_1/D = 60.4$ to $X_1/D = 94.5$, was surrounded by a constant temperature steam bath at 373 K (100 °C). The rib-roughened wall shown in Fig. 1 was generated by machining square ribs, 1 mm × 1 mm in cross-section, directly on one wall with a periodic spacing of 10 mm between adjacent ribs over the length of the duct. Measurements were made in the duct cross-section near the end of the duct midway between adjacent ribs (at $X_1/D = 93.4$) where both the mean temperature and mean velocity fields were fully developed. The operating Reynolds number was 6.5×10^4 based on properties evaluated at the entrance of the heated section.

3. Mathematical model

3.1. Flow field model

Inasmuch as the above flow situation corresponds to incompressible flow with essentially constant thermophysical properties, the mean velocity and Reynolds stress fields were solved first by numerical solution of the boundary layer forms of the conservation equations for mass and momentum in conjunction with reduced forms of the transport equations for k and ε applicable to fully developed rectangular duct flow (cf. Demuren and Rodi, 1984). An algebraic Reynolds stress model was developed to effect closure by considering the exact form of the Reynolds stress transport equations, namely

$$\frac{D\overline{u_iu_j}}{Dt} = -\left(\overline{u_iu_k}\frac{\partial U_j}{\partial X_k} + \overline{u_ju_k}\frac{\partial U_i}{\partial X_k}\right) + \overline{\frac{p}{\rho}\left(\frac{\partial u_i}{\partial X_j} + \frac{\partial u_j}{\partial X_i}\right)} - \frac{\partial}{\partial X_k}\left\{\overline{u_iu_ju_k} - \nu\frac{\partial \overline{u_iu_j}}{\partial X_k} + \overline{\frac{p}{\rho}\left(\delta_{jk}u_i + \delta_{ik}u_j\right)}\right\} - 2\nu\overline{\frac{\partial u_i}{\partial X_k}\frac{\partial u_j}{\partial X_k}}. \quad (1)$$

The convection and diffusion terms in the above equation were modeled using Rodi's approximation, i.e.,

$$\frac{D\overline{u_iu_j}}{Dt} - \mathrm{Diff}_{ij} = \frac{\overline{u_iu_j}}{2k}(P_k - \varepsilon), \quad (2)$$

where Diff_{ij} corresponds to the third term on the right-hand side of Eq. (1). The second (pressure–strain) term on the right-hand side was modeled as a linear combination of the π groups shown in Table 1 which correspond to Rotta's linear return to isotropy model ($\pi_{ij,1} + \pi_{ji,1}$) and the models proposed by Sugiyama et al. (1991) for simulating mean strain rate ($\pi_{ij,2} + \pi_{ji,2}$) and wall proximity ($\pi_{ij,\mathrm{w}} + \pi_{ji,\mathrm{w}}$) effects. The coefficient values specified in Table 2 are the same as those prescribed by Sugiyama et al. (1995) in previous related calculations. Inasmuch as wall functions were used in the present study for the computations, the dissipation rate everywhere in the computed flow was assumed to be locally isotropic, i.e.

$$\varepsilon_{ij} = 2\nu\overline{\frac{\partial u_i}{\partial X_k}\frac{\partial u_j}{\partial X_k}} = \frac{2}{3}\delta_{ij}\varepsilon. \quad (3)$$

The above-specified turbulence model has been successfully applied by Sugiyama et al. (1995) to predict the mean flow and Reynolds stress fields in a square duct with one roughened wall for the same operating conditions as those considered in the present study. Accordingly, these results were used as input for the present calculations, which focus on the mean temperature and turbulent heat flux fields, as calculated by means of two different turbulent heat flux models.

Table 1
Modeling of the pressure–strain correlation term

$\pi_{ij,1} + \pi_{ji,1}$	$-C_1\frac{\varepsilon}{k}\left(\overline{u_iu_j} - \frac{2}{3}k\delta_{ij}\right)$
$\pi_{ij,2} + \pi_{ji,2}$	$-\frac{C_2+8}{11}\left(P_{ij} - \frac{2}{3}P_k\delta_{ij}\right) + \zeta k\left(\frac{\partial U_i}{\partial x_j} + \frac{\partial U_j}{\partial x_i}\right) - \frac{8C_2-2}{11}\left(D_{ij} - \frac{2}{3}P_k\delta_{ij}\right)$
$[\pi_{ij} + \pi_{ji}]_{\mathrm{w}}$	$C_1 = C_1^* + C_1' f\left(\frac{L}{X_{\mathrm{w}}}\right) \quad C_2 = C_2^* + C_2' f\left(\frac{L}{X_{\mathrm{w}}}\right) \quad \zeta = \zeta^* + \zeta' f\left(\frac{L}{X_{\mathrm{w}}}\right)$
$P_{ij} = -\overline{u_iu_k}\frac{\partial U_j}{\partial x_k} - \overline{u_ju_k}\frac{\partial U_i}{\partial x_k} \quad D_{ij} = -\overline{u_iu_k}\frac{\partial U_k}{\partial x_j} - \overline{u_ju_k}\frac{\partial U_k}{\partial x_i}, \quad P_k = -\overline{u_ku_l}\frac{\partial U_k}{\partial x_l}, \quad f\left(\frac{L}{X_{\mathrm{w}}}\right) = \frac{C_\mu^{3/4}}{\kappa}\frac{k^{3/2}}{\varepsilon}\frac{1}{X_{\mathrm{w}}}$	

Table 2
Model constants of the pressure–strain correlation term

C_1^*	C_2^*	ζ^*	C_1'	C_2'	ζ'	C_μ	κ
1.4	0.44	−0.16	−0.35	0.12	−0.1	0.09	0.42

3.2. Temperature field model

The mean temperature and turbulent heat flux fields were calculated from the boundary layer form of the thermal energy equation in conjunction with two algebraic models for the turbulent heat flux correlation which appears in this equation. The development of these models starts with the exact form of the turbulent heat flux transport equation, namely

$$\frac{D\overline{u_iT'}}{Dt} = -\left(\overline{u_iu_j}\frac{\partial T}{\partial X_j} + \overline{u_jT'}\frac{\partial U_i}{\partial X_j}\right) + \overline{\frac{p}{\rho}\left(\frac{\partial T'}{\partial X_i}\right)} - \frac{\partial}{\partial X_j}\left(\overline{u_iu_jT'} + \overline{\frac{p}{\rho}T'\delta_{ij}}\right) - (\nu + a)\overline{\frac{\partial T'}{\partial X_j}\frac{\partial u_i}{\partial X_j}}, \quad (4)$$

where the terms on the right-hand side represent, respectively, the production of turbulent heat flux from the mean flow, the pressure–temperature gradient effect which leads to inhomogeneity among the individual heat flux components, the diffusion of turbulent heat flux, and its dissipation. The convection and diffusion terms were modeled in a manner similar to Rodi's approximation for similar terms that appear in the Reynolds stress transport equation, namely

$$\frac{D\overline{u_iT'}}{Dt} - \mathrm{Diff}_{iT} = \frac{\overline{u_iT'}}{2k}(P_k - \varepsilon), \quad (5)$$

where Diff_{iT} corresponds to the third term on the right-hand side of Eq. (4). The fourth (dissipation) term on the right-hand side of Eq. (4) was neglected on the basis of assumed high Reynolds number flow. The remaining (pressure–temperature gradient) term in Eq. (5) was modeled in two different ways, as described in the following sections.

3.3. Lumley–Launder model

For the flow situation under consideration, the pressure–temperature gradient term can be expressed (exactly) as

$$\overline{\frac{p}{\rho}\frac{\partial T'}{\partial X_i}} = \frac{1}{4\pi}\int\left\{\overline{\left(\frac{\partial^2 u_l u_m}{\partial X_l \partial X_m}\right)'\frac{\partial T'}{\partial X_i}} + 2\left(\frac{\partial U_l}{\partial X_m}\right)'\overline{\left(\frac{\partial u_m}{\partial X_l}\right)'\frac{\partial T'}{\partial X_i}}\right\} \times \frac{dvol}{\left|\mathbf{X} - \mathbf{X}'\right|}, \quad (6)$$

where the prime around quantities in parentheses on the right-hand side denotes quantities evaluated at $\mathbf{X}'$, which is displaced from $\boldsymbol{X}$ by separation distance $\mathbf{r}$. The first and second parts of the integral, defined respectively as $\pi_{iT,1}$ and $\pi_{iT,2}$, represent the effects of pressure–temperature gradient interactions which lead, respectively, to slow and rapid return of the turbulent heat flux components to an isotropic state. In reference to modeling slow return effects, Lumley (1975) modified the model presented by Monin (1965) by introducing an anisotropic tensor into the model coefficients which yielded the following expression for $\pi_{iT,1}$:

$$\pi_{iT,1} = -c_{1T}\frac{\varepsilon}{k}\overline{u_iT'} - c_{1T}'\frac{\varepsilon}{k}\left(\frac{\overline{u_iu_j}}{k} - \frac{2}{3}\delta_{ij}\right)\overline{u_jT'}. \quad (7)$$

In order to model rapid return effects, the following model proposed by Lumley (1975) and independently by Launder (1975) was adopted

$$\pi_{iT,2} = c_{2T}\overline{u_mT'}\frac{\partial U_i}{\partial X_m} - c_{2T}'\overline{u_mT'}\frac{\partial U_m}{\partial X_i}. \quad (8)$$

Inasmuch as wall effects on the model coefficients in Eqs. (7) and (8) are important in the present study, coefficient values were evaluated from the following expressions which take into account wall proximity effects:

$$\begin{aligned} c_{1T} &= c_{1T}^*\left\{1 + c_{1T,\mathrm{w}}f\left(\frac{L}{X_\mathrm{w}}\right)\right\},\\ c_{1T}' &= c_{1T}'^*\left\{1 + c_{1T,\mathrm{w}}f\left(\frac{L}{X_\mathrm{w}}\right)\right\},\\ c_{2T} &= c_{2T}^*\left\{1 + c_{2T,\mathrm{w}}f\left(\frac{L}{X_\mathrm{w}}\right)\right\},\\ c_{2T}' &= c_{2T}'^*\left\{1 + c_{2T,\mathrm{w}}f\left(\frac{L}{X_\mathrm{w}}\right)\right\}, \end{aligned} \quad (9)$$

where X_w is the length perpendicular to the nearest wall and $f(L/X_\mathrm{w})$ is as defined in Table 1. The coefficients with an asterisk in Eq. (9) were selected as $c_{1T}^* = 3.9$, $c_{1T}'^* = -2.5$, which are close to the values specified by Launder (1976) (3.8 and −2.2), and as $c_{2T}^* = 0.8$, $c_{2T}'^* = 0.2$, which correspond to the values selected by Lumley (1975) and Launder (1975). The wall coefficients were specified as $c_{1T,\mathrm{w}} = 0.25$, and $c_{2T,\mathrm{w}} = -0.46$ from comparisons with near-wall turbulence data for an assumed turbulent Prandtl number of 0.92. The slightly different selected values for c_{1T}^* and $c_{1T}'^*$ from those proposed by Launder (1976) led to improved agreement between predictions and experiment in the present study when the composite model given by Eqs. (7)–(9) was employed, which is designated as the Lumley–Launder (LL) model in subsequent discussion.

3.4. Jones–Musonge model

If the pressure–temperature diffusion effects are neglected in Eq. (4), then the temperature–pressure gradient model developed by Jones and Musonge (JM model) is equivalent to a pressure–temperature gradient model that can serve as an alternative to the LL model described in the previous section, i.e.,

$$\overline{\frac{p}{\rho}\frac{\partial T'}{\partial X_i}} = -\overline{\frac{T'}{\rho}\frac{\partial p}{\partial X_i}} = \frac{c_{\phi 1}}{1 + c'_{\phi 1}\sqrt{b_{lm}b_{lm}}}\frac{\varepsilon}{k}\overline{u_i T'} + 2c_{\phi 2}b_{ij}k\frac{\partial T}{\partial X_j} + d_{ijk}\frac{\partial U_j}{\partial X_k}, \tag{10}$$

where

$$d_{ijk} = c_{\phi 3}\delta_{ij}\overline{u_k T'} + c_{\phi 4}\delta_{ik}\overline{u_j T'} + c_{\phi 5}\delta_{jk}\overline{u_i T'}$$

and

$$b_{ij} = \frac{\overline{u_i u_j}}{2k} - \frac{1}{3}\delta_{ij}.$$

The selected values for the model coefficients are the same as those specified by Jones and Musonge, namely: $c_{\phi 1} = c'_{\phi 2} = 3.0$, $c_{\phi 2} = 0.12$, $c_{\phi 3} = 1.09$, $c_{\phi 4} = 0.51$ and $c_{\phi 5} = 0$, where the zero value shown for $c_{\phi 5}$ is compatible with Eq. (10) when $j = k$, a condition corresponding to incompressible flow. These values for the model coefficients were maintained constant in the computations (to observe the predictive capabilities of the JM model in its original form), so that wall proximity effects were not taken into account in applying this model.

4. Numerical method

Inasmuch as the cross-section of the square duct is symmetric about the plane $X_2 = 0$ (refer to Fig. 1), the calculations were performed relative to half of the duct cross-section. Fully developed flow and heat transfer in a smooth walled duct with one roughened wall was assumed. The operating Reynolds number was specified as 6.5×10^4 and all duct walls were assumed to be at the same constant temperature. These conditions correspond to the experimental operating conditions of Hirota et al. (1994, 1997), whose data are used for purposes of comparison in this study. Computations were performed relative to a 22×44 uniform grid in the duct half cross section, with the first grid line near each wall located in the log-law layer, as confirmed by comparison with the data of Hirota et al. (1994). In the present study, the velocity field was calculated first, and then the temperature field, using velocity field results as input for the temperature field calculations. This procedure presumes that the velocity field is unaffected by heated flow conditions, an assumption justified by the isovelocity contours presented by Hirota et al. (1994) which are essentially coincident for isothermal and heated conditions (cf. Fig. 3 in that paper).

The conventional wall functions for k and ε were specified along the first grid line near each wall. On the line adjacent to the roughened wall, the log-law velocity distribution measured by Fujita et al. (1988) was applied, namely

$$\frac{U_1}{U_\tau} = \frac{1}{0.42}\ln\left(\frac{U_\tau y}{\nu}\right) - 8.4, \tag{11}$$

which also was applied at grid points on the corner bisector near each smooth/rough wall intersection. The coefficient −8.4 in Eq. (11) presumes that flow over the roughened wall corresponds to the completely rough flow regime ($U_\tau h/\nu > 100$; cf. Schlichting, 1987, Fig. 20.21). This condition was satisfied, inasmuch as $U_\tau h/\nu$ varied from 100.9 to 125.2 over the duct half width for the computational grid and operating conditions of this study. Along the first grid line adjacent to each smooth wall, the conventional form of the log-law was specified; i.e.,

$$\frac{U_1}{U_\tau} = \frac{1}{0.42}\ln\left(\frac{U_\tau y}{\nu}\right) + 5.5. \tag{12}$$

In the numerical calculations a staggered grid was used and the convection terms in the governing equations were discretized by means of QUICK (third-order upwind differencing). The diffusion terms in the turbulence kinetic energy and dissipation rate equations were discretized by applying power law differencing scheme (PLDS). The solution of the pressure field was obtained by making use of SIMPLE which enabled the mean pressure and velocity fields to be determined through repeat calculations until continuity was satisfied. Further details of the computational procedure are given in the thesis by Matsumoto (1993).

5. Results and discussion

5.1. Mean velocity distributions

Although comparisons between predicted and measured mean velocity distributions have already been presented in an earlier paper (Sugiyama et al., 1995), primary and secondary flow velocity distributions are shown in Figs. 2 and 3, respectively, in order to demonstrate the effect of one roughened wall on the cross-sectioned mean flow pattern in a square duct for fully developed flow conditions. In Fig. 2 contour values of the primary flow velocity component U_1 are normalized by the axial centerline velocity U_c. The secondary flow velocity vectors in Fig. 3 represent the vector sum of U_2 and U_3 normalized by U_c. The dashed line above the lower wall in both figures represents the height of the ribs in the experiments of Hirota et al. (1994, 1997). Fig. 2 shows that predicted primary velocity contours are in relatively good agreement with their experimental counterparts over much of the duct cross-section, except in the central region where predicted contour levels slightly exceed experimental values. The secondary flow velocity vectors in Fig. 3 shows that the experimentally observed, large counter-clockwise cell is simulated well

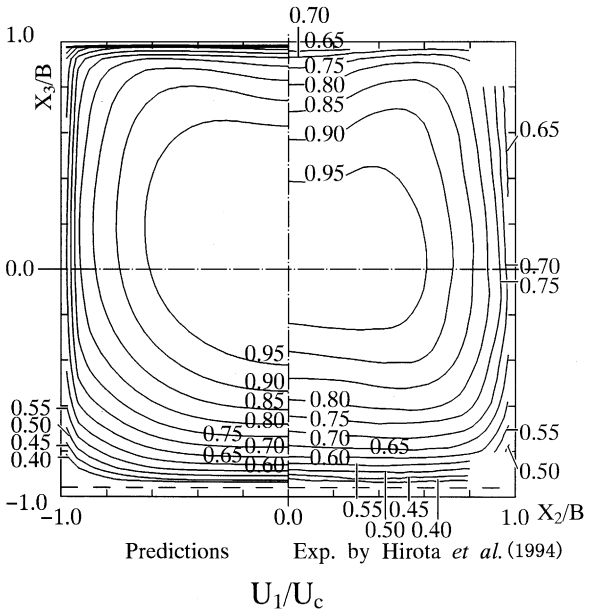

Fig. 2. Primary flow velocity contours.

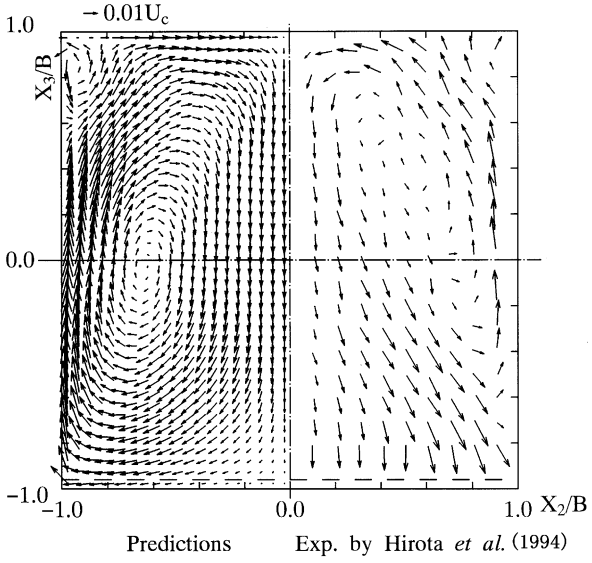

Fig. 3. Secondary flow velocity vectors.

by the predictions. The computations also show, however, that a much smaller counter-rotating cell is predicted near the corner where adjacent smooth walls intersect (at $X_2/B = -1.0$, $X_3/B = 1.0$). This cell is not readily evident in the experimental pattern. It should be noted, however, that Naimi and Gessner (1997) have shown that this small cell is also predicted when alternate turbulence models are employed, namely the k–ε transport equation model proposed by Demuren and Rodi (1984), and the Reynolds stress transport equation model developed by Naimi and Gessner (1995). It would appear, therefore, that the small cell observed in the predictions of Fig. 3 is a real effect.

5.2. Mean temperature distributions

Mean temperature contours calculated by applying the LL and JM turbulent heat flux models are compared with experimental contours in Figs. 4 and 5, where the temperature difference $T_w - T$ is normalized by $T_w - T_c$, with T_w and T_c defined as (uniform) wall temperature and axial centerline temperature, respectively. A comparison of these two figures shows that

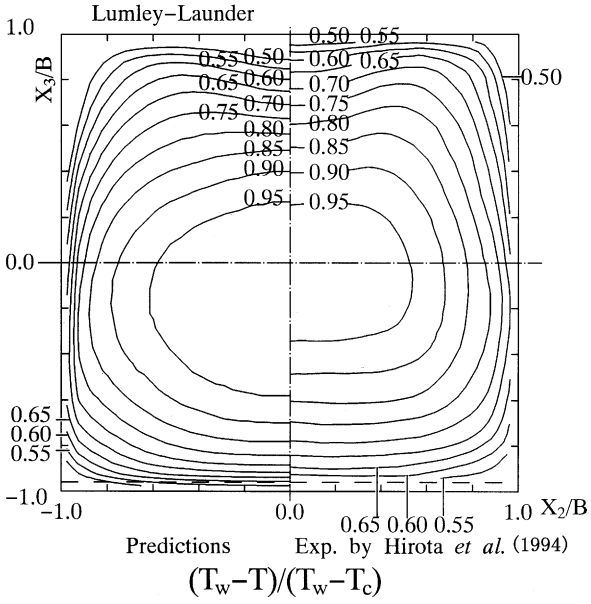

Fig. 4. Mean temperature contours: LL model predictions and experiment.

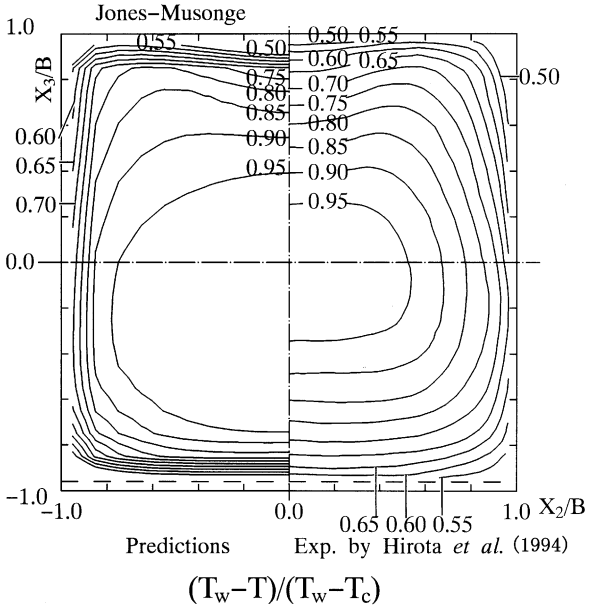

Fig. 5. Mean temperature contours: JM model predictions and experiment.

results based on the LL model are in better agreement with experiment than results based on the JM model. In reference to Fig. 5, application of the JM model leads to relatively uniform temperatures in the central portion of the duct and to steep temperature gradients near opposite smooth and rough walls which are not present in the experiment flow. A possible reason for this behavior is that the heat flux model proposed by Jones and Musonge (1988) does not include wall effects in its formulation, as noted earlier, which may account, in part, for the discrepancies between predictions and experiment seen in Fig. 5.

5.3. Turbulent heat flux distributions

Figs. 6 and 7 compare LL and JM model predictions of the turbulent heat flux component $\overline{u_1T'}$ with experimental results obtained by Hirota et al. (1997). In general, both models tend to overpredict contour levels in the upper half of the duct ($0 \leqslant X_3/B \leqslant 1$) and underpredict contour levels in the lower half of the duct ($-1 \leqslant X_3/B \leqslant 0$). In the immediate vicinity of lower roughened wall, contour levels predicted by the LL model are in relatively good agreement with experimental levels (Fig. 6), but contour levels predicted by the JM model are excessively high (Fig. 7). In contrast, Fig. 7 also shows that the JM model leads to predicted $\overline{u_1T'}$ levels in the central region of the duct that are excessively low in comparison to their experimental counterparts. This shortcoming applies to a lesser extent to the results shown in Fig. 6. It should also be noted that neither the LL model nor the JM model is able to simulate experimentally observed contour behavior in the octant between the roughened wall and the bisector of the corner formed by this wall and the adjacent smooth wall. More specifically, neither model is able to simulate the observed peaking characteristic of experimental contours near the roughened wall.

Predicted contours of the turbulent heat flux component $\overline{u_2T'}$ are compared with the experimental results of Hirota et al. (1997) in Figs. 8 and 9. In general, there is fair agreement between predicted and

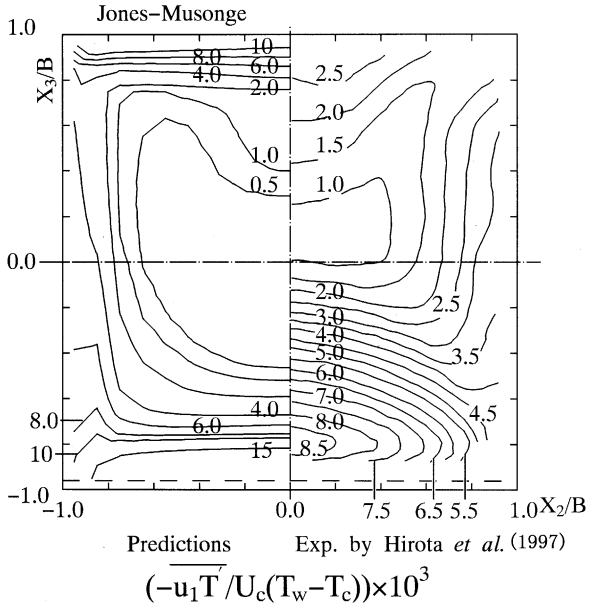

Fig. 7. Turbulent heat flux component $-\overline{u_1T'}$ contours: JM model predictions and experiment.

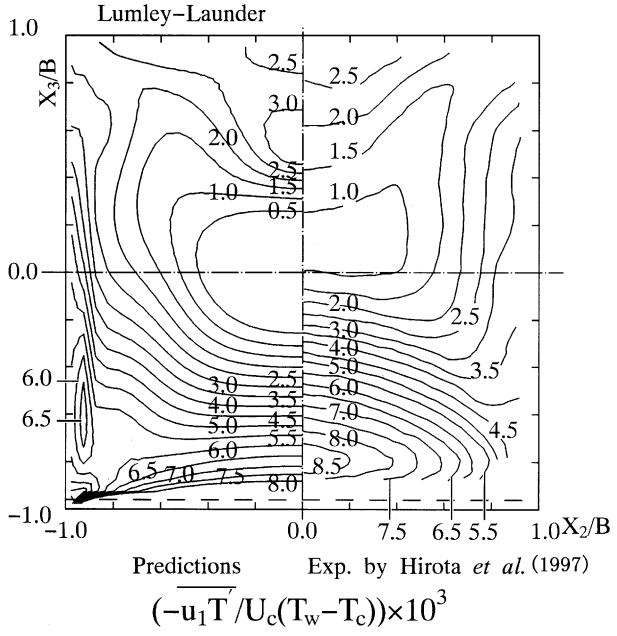

Fig. 6. Turbulent heat flux component $-\overline{u_1T'}$ contours: LL model predictions and experiment.

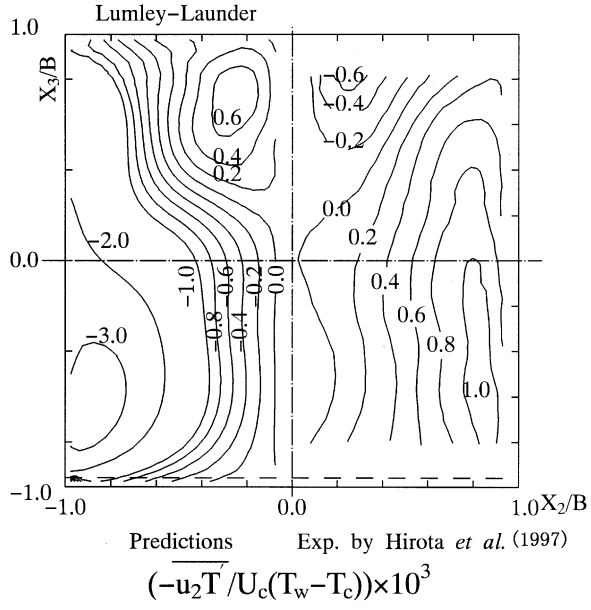

Fig. 8. Turbulent heat flux component $-\overline{u_2T'}$ contours: LL model predictions and experiment.

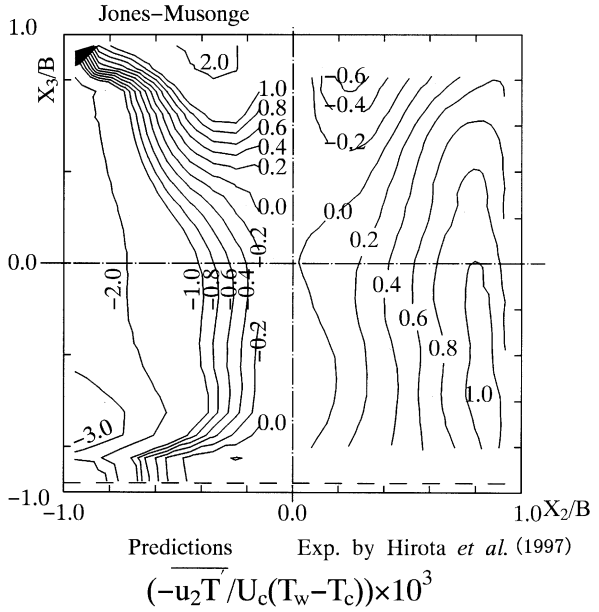

Fig. 9. Turbulent heat flux component $-\overline{u_2T'}$ contours: JM model predictions and experiment.

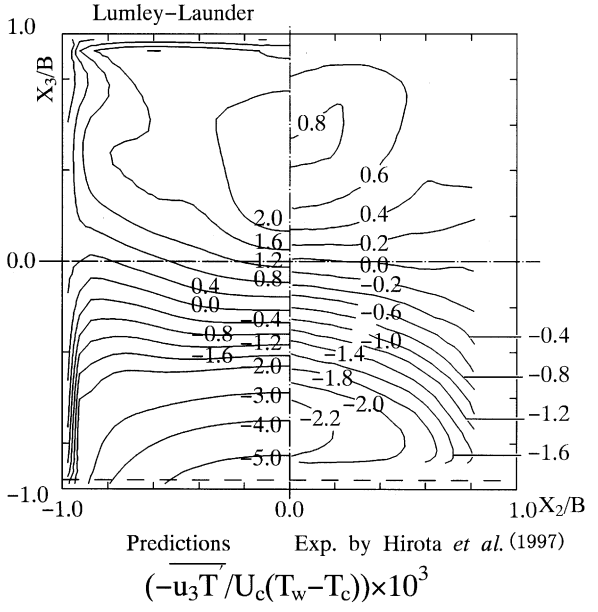

Fig. 10. Turbulent heat flux component $-\overline{u_3T'}$ contours: LL model predictions and experiment.

experimental contour levels, with both models leading to steeper gradients than those observed experimentally. In particular, the JM model leads to very steep $\overline{u_2T'}$ gradients near the intersection of adjacent smooth walls (at $X_2/B = -1.0$, $X_3/B = 1.0$) that are not present in the experimental flow. Both models are also unable to simulate the experimentally observed peaking characteristic of contours measured near the side wall. The experimental results near the smooth wall opposite the roughened wall appear to indicate the presence of a closed contour pattern, an effect simulated well by the LL model, but not by the JM model.

Experimentally measured $\overline{u_3T'}$ contours are compared with predictions by the LL and JM models in Figs. 10 and 11, respectively. The experimental contours show that $\overline{u_3T'}$ changes sign in the X_3 (vertical) direction, with the zero line nominally aligned with horizontal bisector of the duct cross-section ($X_3 = 0$). This behavior is predicted relatively well by the LL model, in comparison to the JM model, which predicts the zero line location as being midway between the horizontal bisector and the roughened wall. As a result, the JM model predicts positive values of $\overline{u_3T'}$ in the lower half at the duct, a region where all experimental values are negative. Both the LL and JM models tends to overpredict $\overline{u_3T'}$ values in the upper half of the duct, and negative contour levels predicted by the LL model near the roughened wall are larger in magnitude than experimentally observed values. On balance, however, the LL model, in comparison to the JM model, predicts contours that are in better overall agreement with the data.

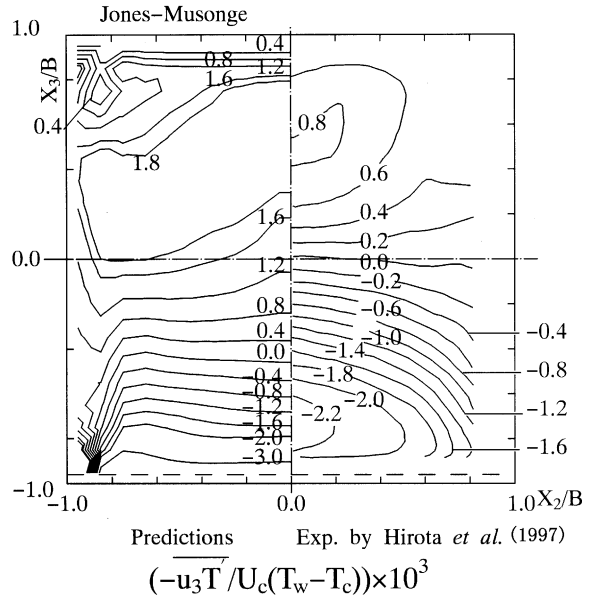

Fig. 11. Turbulent heat flux component $-\overline{u_3T'}$ contours: JM model predictions and experiment.

6. Conclusions

The predictive capabilities of two algebraic turbulent heat flux models have been analyzed by means of comparisons with data obtained for fully developed flow and heat transfer in a square duct having one roughened wall and with all four walls maintained at a constant elevated temperature. Two models for the pressure–temperature gradient term in the turbulent heat flux transport equation were considered, namely the LL model, as

defined in this study, and JM model, as originally formulated by the authors. One of the main differences between these two models is that the LL model includes near-wall effects in its formulation, whereas the JM model does not. On the basis of the comparisons made in this study, it was found that the LL model performed better than the JM model, not only with respect to predicting turbulent heat flux component behavior, but also with respect to predicting the mean temperature field. Discrepancies still exist, however, between predictions and experiment which demonstrate the need for further work in this area. These include the inability of either model to predict the experimentally observed peaking characteristic of $\overline{u_1 T'}$ near the roughened wall and of $\overline{u_2 T'}$ near the adjacent side wall. Both models also predict gradients of $\overline{u_2 T'}$ in the duct cross-section which are much steeper than their experimental counterparts. Contour levels of $\overline{u_3 T'}$ predicted by both models are in fair agreement with experimental values, and change sign to follow the data, but the zero line location is not predicted well by either model, with the JM model yielding the greatest discrepancy.

Acknowledgements

The authors would like to thank the Japanese Ministry of Education for providing funds (Grant-in-Aid for Scientific Research, C, No. 10650198) to support this study.

References

Demuren, A.O., Rodi, W., 1984. Calculation of turbulence-driven secondary motion in non-circular ducts. J. Fluid Mech. 140, 189–222.

Fujita, H., Yokosawa, H., Hirota, M., Nagata, C., 1988. Fully developed flow and heat transfer in a square duct with two roughened facing walls. Chem. Eng. Comm. 74, 95–110.

Fujita, H., Yokosawa, H., Hirota, M., 1989. Secondary flow of the second kind in rectangular ducts with one rough wall. Exp. Therm. Fluid Sci. 2 (1), 72–80.

Fujita, H., Hirota, M., Yokosawa, H., 1990. Experiments on turbulent flow in a square duct with a rough wall. Memoirs of the Faculty of Engineering, Nagoya University 41 (2), 280–294.

Gessner, F.B., Eppich, H.M., 1981. A near-wall pressure strain model for turbulent corner flows. In: Proceedings of the 3rd Symposium on Turbulent Shear Flows, University of California, Davis, pp. 2.25–2.32.

Hirota, M., Fujita, H., Yokosawa, H., 1994. Experimental study on convective heat transfer for turbulent flow in a square duct with a ribbed rough wall (characteristics of mean temperature field). J. Heat Trans., Trans. ASME 116 (5), 332–340.

Hirota, M., Fujita, H., Itakura, S., Yuasa, H., 1997. Turbulent heat transfer in square ducts with rough walls. In: Proceedings of the 34th National Heat Transfer Conference, pp. 347–348 (in Japanese).

Humphrey, J.A.C., Whitelaw, J.H., 1980. Turbulent flow in a duct with roughness. In: Turbulent Shear Flows, 2. Springer, Berlin, pp. 174–188.

Jones, W.P., Musonge, P., 1988. Closure of the Reynolds stress and scalar flux equations. Phys. Fluids 31 (12), 3589–3604.

Launder, B.E., 1975. Progress in the modelling of turbulent transport. In: Prediction Methods for Turbulent Flow. Lecture Series 76, von Karman Inst., Belgium.

Launder, B.E., 1976. Heat and mass transport. In: Turbulence, Topics in Applied Physics, 12. Springer, Berlin, pp. 231–287.

Lumley, J.L., 1975. Introduction. In: Prediction Methods for Turbulent Flows. Lecture Series 76, von Karman Inst., Belgium.

Matsumoto, M., 1993. Numerical simulation of turbulent structure and heat transfer in square duct with roughened wall. M.S. thesis, Department of Mechanical Engineering, Utsunomiya University, Japan (in Japanese).

Monin, A.S., 1965. On the symmetry properties of turbulence in the surface layer of air. Atmos. Oceanic Phys. 1 (1), 25–30.

Naimi, M., Gessner, F.B., 1995. A calculation method for developing turbulent flow in rectangular ducts of arbitrary aspect ratio. J. Fluids Eng., Trans. ASME 117 (6), 249–258.

Naimi, M., Gessner, F.B., 1997. Calculation of fully-developed turbulent flow in rectangular ducts with non-uniform wall roughness. J. Fluids Eng., Trans. ASME 119 (3), 550–558.

Rodi, W., 1976. A new algebraic relation for calculating the Reynolds stresses. ZAMM (56), T219–T221.

Schlichting, H., 1987. In: Boundary-Layer Theory, seventh ed. McGraw-Hill, New York, p. 620.

Sugiyama, H., Akiyama, M., Serizawa, T., 1991. Numerical analysis of developing flow in a square duct using Reynolds stress model. In: Proceedings of the ASME/JSME Thermal Engineering, 3. ASME, New York, pp. 159–165.

Sugiyama, H., Akiyama, M., Matsumoto, M., Hirata, M., Ninomiya, N., 1993. Numerical analysis of fully developed turbulent flow in a square duct with a rough wall. Trans. JSME 59 (561), 1510–1517 (in Japanese).

Sugiyama, H., Akiyama, M., Matsumoto, M., 1995. Numerical analysis of turbulent structure and heat transfer in a square duct. In: Proceedings of the ASME/JSME Thermal Engineering, Book No. H0933A. ASME, New York, pp. 409–416.

Yokosawa, H., Fujita, H., Hirota, M., Iwata, S., 1989. Measurement of turbulent flow in a square duct with roughened walls on two opposite sides. Int. J. Heat Fluid Flow 10 (2), 125–130.